PAPER

Check for updates

Synthesis of macro-rotaxanes *via* direct trapping of multicyclic poly(*n*-butyl acrylate) in a cross-linked network

Kotaro Ibe,[a] Yamato Ebii,[a] Minami Ebe, [b] Kazushige Suzuki,[b]
Takayuki Kurokawa, [c] Takuya Yamamoto, [b] Feng Li, [b] Takuya Isono [*b] and
Toshifumi Satoh [*b,d,e]

Macro-rotaxanes, in which both the linear and cyclic components are polymers, remain largely unexplored in terms of their formation and potential material applications due to the synthetic challenges associated with cyclic polymers. In this study, macro-rotaxane formation was investigated by means of the photoradical polymerization of *n*-butyl acrylate (BA) and a cross-linker in the presence of multicyclic poly(*n*-butyl acrylate) (mc-PBA). For this purpose, mc-PBAs with different average numbers of cyclic units (N_{ring}) and cyclic unit molecular weights ($M_{n,ring}$) were synthesized *via* the cyclopolymerization of an α,ω-dinorbornenyl-functionalized PBA macromonomer. Subsequently, polymer networks incorporating mc-PBA were prepared and the trapping efficiency of mc-PBA within these networks was evaluated. The fraction of mc-PBA trapped as the macro-rotaxane increased with increasing N_{ring} and $M_{n,ring}$. Additionally, dynamic viscoelastic measurements revealed that the incorporation of mc-PBA enhanced the damping properties of the resulting PBA networks. Notably, these properties were retained even after the removal of untrapped mc-PBA by solvent washing, demonstrating that mc-PBA functioned effectively as a non-leaching additive.

Introduction

Rotaxanes are supramolecular structures in which a linear molecule penetrates a cyclic component and is stabilized in the presence of bulky stoppers (Fig. 1a). Owing to the presence of such mechanical bonds, rotaxanes exhibit molecular mobility that cannot be achieved through covalent bonding, thereby reflecting one of their most distinctive features. By exploiting the mobility of their cyclic component, rotaxanes have been extensively studied for applications in molecular machines[1–3] and drug delivery systems,[4–6] with interest in these structures recently extending to polymer materials. In particular, the use of topologically cross-linked polymers incorporating rotaxanes

as movable cross-linking points has emerged as an effective strategy for enhancing the mechanical properties of conventional materials owing to their superior stress dissipation capability.[7–9]

Various strategies for constructing rotaxanes have been reported, most of which employ small cyclic molecules, such as crown ethers[10–12] or cyclodextrins,[13–15] as cyclic components. For example, Stoddart *et al.*[10] demonstrated that rotaxanes can be formed by exploiting ion–dipole interactions and hydrogen bonding between crown ethers and ammonium-containing linear components. Additionally, Harada *et al.*[13] established a method in which hydrophobic interactions between cyclodextrins and linear components serve as the driving force for rotaxane formation (Fig. 1b). In principle, the self-assembly of cyclic and linear components to form pseudorotaxanes, which are precursors of rotaxanes, is entropically unfavorable. Thus, strong intermolecular interactions, including ion–dipole interactions, hydrogen bonding, hydrophobic interactions, or π–π stacking,[16–19] are indispensable as driving forces in (pseudo)rotaxane formation. Consequently, the accessible combinations of cyclic and linear components remain limited.

Our group recently investigated a new class of rotaxanes, termed macro-rotaxanes, in which both the linear and cyclic components consist of polymers. In contrast to small-molecule-based

a Graduate School of Chemical Sciences and Engineering, Hokkaido University, Kita 13, Nishi 8, Kita-ku, Sapporo, Hokkaido 060-8628, Japan
b Faculty of Engineering, Hokkaido University, Kita 13, Nishi 8, Kita-ku, Sapporo, Hokkaido 060-8628, Japan. E-mail: isono.t@eng.hokudai.ac.jp, satoh@eng.hokudai.ac.jp
c Division of Soft Matter, Faculty of Advanced Life Science, Hokkaido University, Sapporo 001-0021, Japan
d List Sustainable Digital Transformation Catalyst Collaboration Research Platform, Institute for Chemical Reaction Design and Discovery, Hokkaido University, Kita 21, Nishi 10, Kita-ku, Sapporo, Hokkaido 001-0021, Japan
e Department of Chemical & Materials Engineering, National Central University, Taoyuan 320317, Taiwan
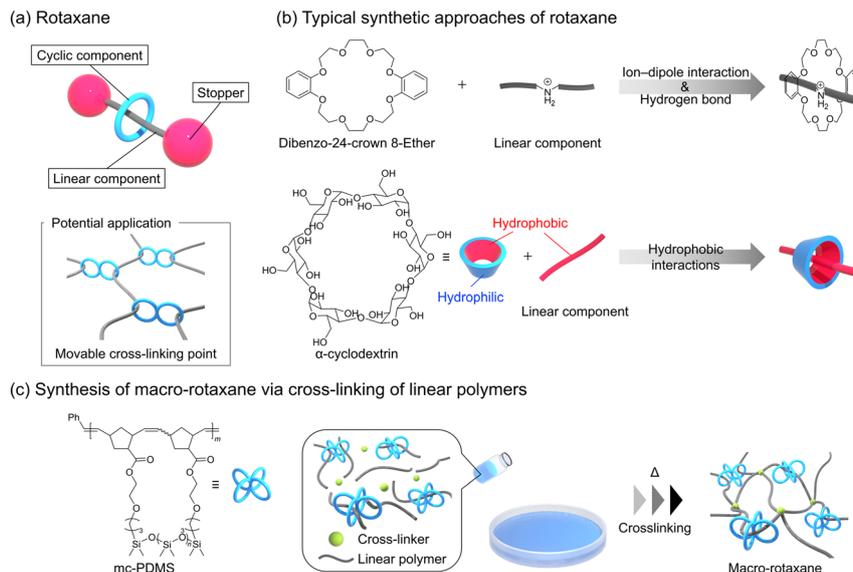
Fig. 1 (a) Schematic representation of the rotaxane structure and its potential application. (b) Typical synthetic strategies for rotaxane formation. (c) Example of macro-rotaxane formation *via* the cross-linking of linear polymers.

rotaxanes, macro-rotaxane formation does not require specific intermolecular attractive interactions to generate the pseudorotaxane, which is expected to allow a broader range of combinations of cyclic and linear components. When both the linear and cyclic components are composed of the same polymer, the linear component spontaneously threads through the polymer ring, resulting in the formation of a pseudomacro-rotaxane. Such spontaneous threading has been supported by both experimental[20,21] and computational studies.[22] From an experimental perspective, it was demonstrated that the addition of a small amount of linear polystyrene (PS) to cyclic PS leads to a substantial increase in viscoelasticity, indicating that cyclic PS acts as a dynamic cross-linking point through threading with the linear PS.[20] In another study,[23] the possibility of pseudomacro-rotaxane formation using a linear polymer in combination with a monocyclic polymer was experimentally suggested using small-angle neutron scattering. Moreover, computational studies based on molecular dynamics simulations further demonstrated that blends of cyclic and linear polymers exhibit a negative Flory–Huggins interaction parameter, indicating that pseudomacro-rotaxane formation could occur spontaneously.[22]

The threading structures generated from cyclic and linear polymers have been discussed historically in terms of "topological trapping".[24–30] For instance, Semlyen *et al.*[24] reported that up to 94% of monocyclic polydimethylsiloxane (PDMS) molecules were trapped within a polymer network *via* the cross-linking of end-functionalized PDMS chains. Additionally, Waymouth *et al.*[25] performed the radical polymerization of 2-hydroxyethyl methacrylate in the presence of monocyclic poly(alkylene phosphate), revealing that 36% of the cyclic polymer was incorporated into the resulting network. These networks satisfy the structural requirements for a rotaxane architecture, wherein the cross-linking points serve as stoppers to produce macro-rotaxanes. Although such macro-rotaxanes

have been realized in practice, studies have primarily focused on assessing the presence and formation efficiency of cyclic polymers, and their potential as functional material components remains largely unexplored. This stems from the fact that previous studies have primarily focused on developing cyclic polymer synthesis methods rather than investigating the material properties.

Our group previously reported a cyclopolymerization approach for the facile synthesis of various well-defined multicyclic polymers, in which linear macromonomers functionalized at both ends underwent successive reactions to generate multiple rings in a single step.[31] This method relies on ring-opening metathesis polymerization (ROMP) initiated by a third-generation Grubbs catalyst (G3), which serves as the elementary ring-forming process. Specifically, α,ω-dinorbornenyl-functionalized linear polymers were employed as macromonomers, and ROMP conducted under high-dilution conditions promoted alternating intramolecular cyclization and intermolecular propagation to afford well-defined multicyclic architectures. This approach was applicable to a wide variety of polymer species, including poly(L-lactic acid), PDMS,[32] and PS.[33]

Furthermore, by combining this facile cyclopolymerization approach with topological trapping based on the cross-linking of linear polymers, our group demonstrated that macro-rotaxanes can be efficiently formed when multicyclic PDMS (mc-PDMS) is employed as the cyclic component (Fig. 1c).[32] These results provided concrete experimental validation of the macro-rotaxane concept. Remarkably, mc-PDMS exhibited superior efficiency in macro-rotaxane formation compared with its monocyclic counterpart. Additionally, using coarse-grained molecular dynamics simulations, Hagita *et al.*[34] demonstrated that the extent of linear polymer threading increased from monocyclic to bicyclic and tricyclic polymers. Beyond the fundamental interest in macro-rotaxane formation,

the resulting networks were useful as damping materials, as the cyclic components relaxed independently from the cross-linked network. Furthermore, the macro-rotaxanes composed of mc-PDMS toughened the polymer network.[35] These reports demonstrate the advantages of multicyclic polymers as cyclic components for macro-rotaxanes. However, despite such advances, the formation of macro-rotaxanes using multicyclic polymers remains largely unexplored.

The aim of the current study is therefore to extend the scope of this cyclopolymerization approach to the formation of macro-rotaxanes using a method distinct from our previous end-cross-linking strategy, thereby opening additional possibilities for their application (Fig. 2). For this purpose, poly(n-butyl acrylate) (PBA), a polymer widely used in adhesives and damping materials, was selected as the model system. Additionally, α,ω-dinorbornenyl-functionalized PBA (NB–PBA–NB) was used as a macromonomer to synthesize multicyclic PBA (mc-PBA) with varying numbers of cyclic units and molecular weights. Thus, mc-PBA-blended PBA networks, in which mc-PBA was topologically trapped within the cross-linked PBA network, were constructed via the photoradical polymerization of n-butyl acrylate (BA) and a cross-linker in the presence of mc-PBA. Systematic evaluation of the macro-rotaxane formation efficiency was subsequently performed to investigate the influence of different molecular parameters. Furthermore, dynamic viscoelastic measurements were carried out to reveal the effects of mc-PBA on damping properties and as a non-leaching additive to facilitate the development of materials exhibiting stable performance over extended periods.

Results and discussion

Synthesis of the macromonomer

NB–PBA–NB, serving as a macromonomer for mc-PBA, was synthesized via atom transfer radical polymerization (ATRP) of BA, followed by nucleophilic substitution of the bromo-terminals with exo-5-norbornenecarboxylic acid (exo-NB–COOH) (Schemes 1(a) and (b)).

Initially, dibromo-terminated PBA (Br–PBA–Br) was prepared via ATRP, targeting a number-average molecular weight (M_n) of ~10 000. Ethylene bis(2-bromoisobutyrate) (EBBiB), copper(I) bromide (CuBr), N,N,N',N'',N''-pentamethyldiethylenetriamine (PMDETA), and copper(II) bromide (CuBr$_2$) were employed as the initiator, catalyst, ligand, and deactivator, respectively ([BA]$_0$/[EBBiB]$_0$/[CuBr]/[CuBr$_2$]/[PMDETA] = 224 : 1.00 : 0.95 : 0.05 : 1.10). Polymerization was conducted in a mixed solvent of anisole and dry N,N-dimethylformamide (DMF) at 70 °C for 2.5 h under an argon atmosphere (Table 1, run 1). The M_n of the resulting Br–PBA–Br was determined by proton nuclear magnetic resonance (^{1}H NMR) spectroscopy ($M_{n,NMR}$), giving a value of 11 600, while size-exclusion chromatography (SEC) using polystyrene standards ($M_{n,SEC}$) yielded a value of 10 400, with a molecular weight dispersity ($Đ$) of 1.07 (Fig. S1 and S2).

Subsequently, NB–PBA–NB was synthesized via the nucleophilic substitution of Br–PBA–Br with exo-NB–COOH. This reaction was carried out according to a previously reported method for similar end-group functionalization of polyacrylates.[36] The reaction was performed at room temperature in dry DMF for 166 h, employing 1,8-diazabicyclo[5.4.0]-7-undecene (DBU) as the base ([Br–PBA–Br]$_0$/[exo-NB–COOH]$_0$/[DBU] = 1.0 : 4.0 : 4.0, [Br–PBA–Br]$_0$ = 100 g L^{-1}; Table 1, run 2). ^{1}H NMR analysis confirmed the quantitative conversion of Br–PBA–Br into NB–PBA–NB, as evidenced by a downfield shift of the chain-end methine protons from 4.29–3.84 to 5.03–4.90 ppm, together with the appearance of characteristic norbornenyl olefinic and bridgehead proton signals at 6.21–6.06 and 3.21–2.88 ppm, respectively. The expected integration ratios were calculated for all characteristic peaks of NB–PBA–NB, confirming sufficient end-group fidelity (Fig. S11). Additionally, SEC revealed a monomodal elution
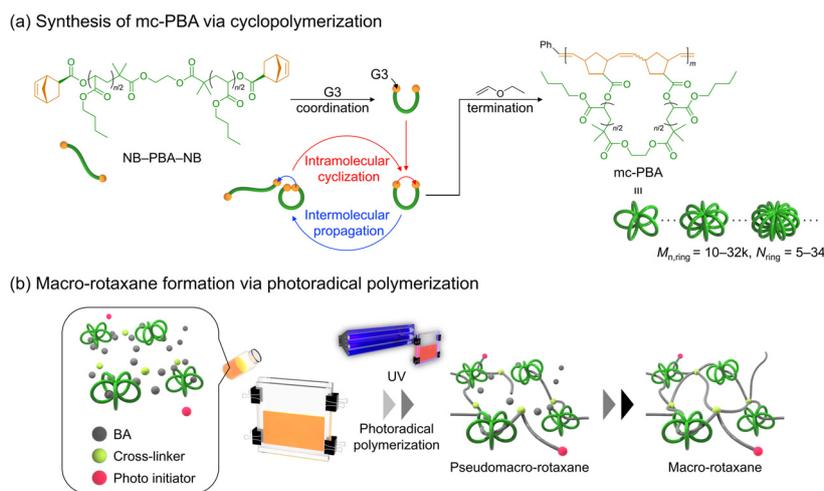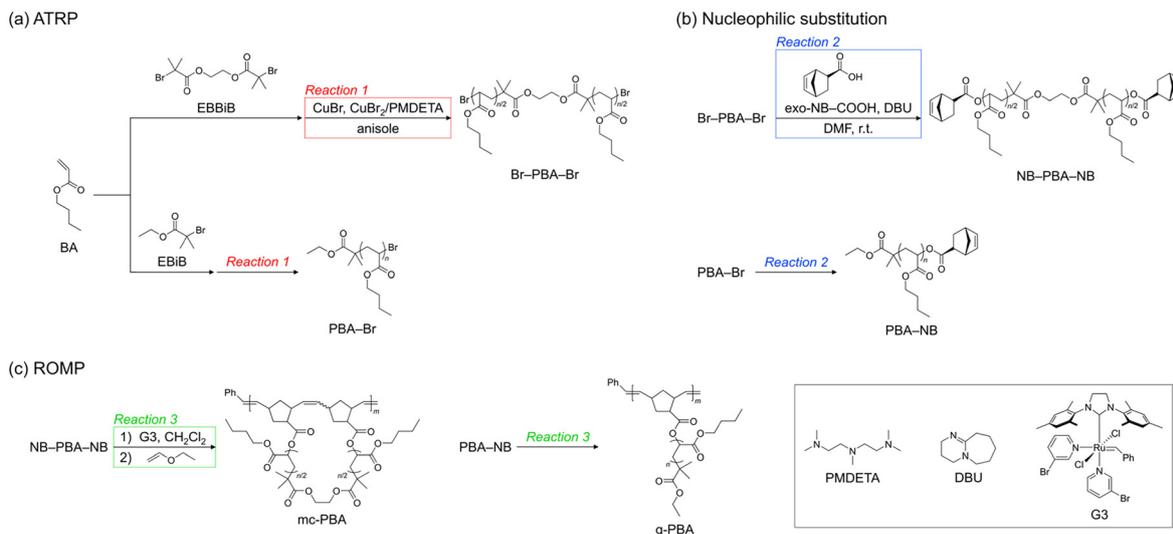

Fig. 2 (a) Synthesis of mc-PBA via cyclopolymerization. (b) Macro-rotaxane formation via photoradical polymerization of BA in the presence of mc-PBA.

Scheme 1 Synthesis of (a) Br–PBA–Br and PBA–Br, (b) NB–PBA–NB and PBA–NB, and (c) mc-PBA and g-PBA.

Table 1 ATRP of BA using EBBiB as an initiator,[a] and subsequent synthesis of NB–PBA–NB[b]

Run	Sample	Time [h]	$M_{n,NMR}$ [c]	$M_{n,SEC}$ [d]	$Đ$ [d]	$M_{n,MALS}$ [e]	$Đ_{MALS}$ [e]
1	Br–PBA$_{10k}$–Br	2.5	11 600	10 400	1.07	—	—
2	NB–PBA$_{10k}$–NB	166	12 000	10 900	1.07	10 200	1.15
3	Br–PBA$_{19k}$–Br	7.0	23 400	20 900	1.07	—	—
4	NB–PBA$_{19k}$–NB	161	24 300	21 500	1.08	19 200	1.05
5	Br–PBA$_{32k}$–Br	13.0	41 900	35 000	1.10	—	—
6	NB–PBA$_{32k}$–NB	138	39 700	37 100	1.10	31 500	1.03

[a] Polymerization conditions: Ar atmosphere; solvent, anisole/DMF; $[BA]_0/[initiator]_0/[CuBr]/[CuBr_2]/[PMDETA]$ = 224 : 1.00 : 0.95 : 0.05 : 1.10 (run 1), 511 : 1.00 : 0.95 : 0.05 : 1.10 (run 3), and 770 : 1.00 : 0.95 : 0.05 : 1.10 (run 5). [b] Reaction conditions: solvent, dry DMF; temperature, r.t.; [Br–PBA–Br]$_0$/[exo-NB–COOH]$_0$/[DBU] = 1.0 : 4.0 : 4.0 (run 2), 1.0 : 4.3 : 4.1 (run 4), and 1.0 : 4.2 : 4.1 (run 6); [Br–PBA–Br]$_0$ = 100 g L^{-1}. [c] Determined by ^{1}H NMR spectroscopy performed in CDCl$_3$ (Fig. S1, S3, S5, S11, S13, and S15). [d] Determined by SEC in THF using PS standards (Fig. S2, S4, S6, S12, S14, and S16). [e] Calculated using multi-angle light scattering.

peak both before and after the reaction, indicating the absence of side reactions and confirming the selective progression of the desired substitution (Fig. S12). The absolute M_n ($M_{n,MALS}$) of the product, determined by SEC coupled with multi-angle light scattering and viscometry (SEC-MALS-Visco), was 10 200. For clarity, the polymers were denoted as Br–PBA$_{10k}$–Br and NB–PBA$_{10k}$–NB, based on the $M_{n,MALS}$ values of NB–PBA–NB. Furthermore, by varying the feed ratios of $[BA]_0/[EBBiB]_0/$ $[CuBr]/[CuBr_2]/[PMDETA]$ and $[Br–PBA–Br]_0/[exo-NB–COOH]_0/$ $[DBU]$, a series of PBA macromonomers with different molecular weights (i.e., 19k and 32k) were synthesized, as summarized in Table 1 (runs 3–6; Fig. S3–S6 and S13–S16).

Synthesis of mc-PBA via cyclopolymerization

mc-PBA was synthesized via the cyclopolymerization of NB–PBA$_{10k}$–NB (Table 2, run 1; Scheme 1c). The reaction was performed under an argon atmosphere in dry CH$_2$Cl$_2$ at room temperature for 3.5 h. To suppress intermolecular reactions and promote intramolecular cyclization, high-dilution conditions were employed, with $[NB–PBA_{10k}–NB]_0$ = 0.11 mmol L^{-1}. To obtain mc-PBA$_{10k}$ containing eight cyclic units, an

$[NB–PBA_{10k}–NB]_0/[G3]_0$ feed ratio of 8 : 1 was used. Even after completion of the reaction, no gelation was observed, and only soluble products were obtained. The SEC profile of the crude product revealed a shoulder peak in the lower-molecular-weight region arising from the mc-PBA species containing fewer cyclic units, which were removed by preparative SEC (Fig. S20). The ^{1}H NMR spectrum of the purified product showed complete disappearance of the signals corresponding to the terminal norbornenyl group of NB–PBA$_{10k}$–NB (H$_a$, H$_b$, 6.21–6.06 ppm; H$_c$, H$_d$, 3.21–2.88 ppm), while the overlapping broad signals (5.62–4.74 and 4.36–2.00 ppm) corresponded to protons of the polynorbornene backbone (Fig. 3a), indicating successful ROMP. SEC demonstrated that the elution peak of the product shifted to a higher-molecular-weight region compared with NB–PBA$_{10k}$–NB ($M_{n,SEC}$ = 48 600, $Đ$ = 1.16), as depicted in Fig. 3b. Subsequently, the average number of cyclic units (N_{ring}) was calculated by dividing the $M_{n,MALS}$ value of mc-PBA by that of NB–PBA–NB. For NB–PBA$_{10k}$–NB, the $M_{n,MALS}$ of mc-PBA was 83 200; therefore, the resulting mc-PBA exhibited an N_{ring} value of ~8 and was denoted as 8c-PBA$_{10k}$. As reported previously, N_{ring} can be tuned by varying the

Table 2 Synthesis of mc-PBA[a]

Run	Sample	Macromonomer	$[MM]_0/[G3]_0$	$[MM]_0$ [mmol L^{-1}]	Time [h]	$M_{n,SEC}$[b]	$Đ$[b]	$M_{n,MALS}$[c]	$Đ_{MALS}$[c]	$M_{n,ring}$[c]	N_{ring}[d]	Yield [%]
1	8c-PBA$_{10k}$	NB–PBA$_{10k}$–NB	8 : 1	0.11	3.5	48 600	1.16	83 200	1.15	10 200	8	69.0
2	34c-PBA$_{10k}$	NB–PBA$_{10k}$–NB	48 : 1	0.11	27.0	110 200	1.34	348 300	1.62	10 200	34	50.0
3	12c-PBA$_{19k}$	NB–PBA$_{19k}$–NB	15 : 1	0.10	27.0	108 300	1.40	222 400	1.75	19 200	12	68.0
4	5c-PBA$_{32k}$	NB–PBA$_{32k}$–NB	4 : 1	0.07	8.5	118 100	1.39	162 100	1.27	31 500	5	61.7
5	8c-PBA$_{32k}$	NB–PBA$_{32k}$–NB	8 : 1	0.07	7.5	159 000	1.43	256 100	1.47	31 500	8	56.0
6	13c-PBA$_{32k}$	NB–PBA$_{32k}$–NB	19 : 1	0.07	25.0	221 700	1.58	403 800	2.38	31 500	13	45.7

[a] Polymerization conditions: solvent, dry CH$_2$Cl$_2$; temperature, r.t. [b] Determined by SEC in THF using PS standards (Fig. S20, S22, S24, S26, S28 and S30). [c] Calculated using multi-angle light scattering. [d] N_{ring} was calculated for the obtained mc-PBA using the expression: ($M_{n,MALS}$ of mc-PBA)/($M_{n,ring}$).
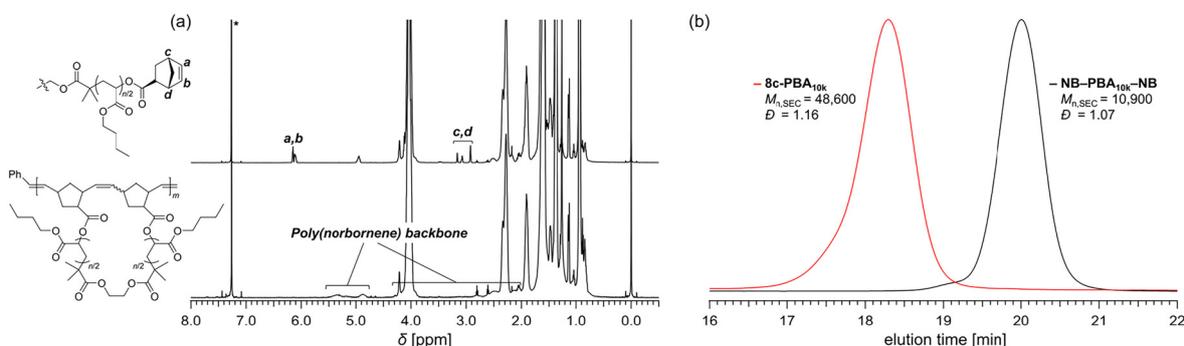

Fig. 3 (a) ^{1}H NMR spectra of NB–PBA$_{10k}$–NB (top) and 8c-PBA$_{10k}$ (bottom) (solvent, CDCl$_3$; 600 MHz). The asterisk denotes the solvent peak. (b) SEC traces of NB–PBA$_{10k}$–NB (black) and 8c-PBA$_{10k}$ (red) (eluent, THF; flow rate, 1.0 mL min^{-1}).

[macromonomer]$_0$/[G3]$_0$ feed ratio during cyclopolymerization. Accordingly, increasing the [NB–PBA$_{10k}$–NB]$_0$/[G3]$_0$ ratio to 48 : 1 enabled the synthesis of mc-PBA$_{10k}$ with a greater N_{ring} (34c-PBA$_{10k}$; $M_{n,MALS}$ = 348 300, $Đ_{MALS}$ = 1.62), as detailed in Table 2 (run 2; Fig. S21 and S22).

To systematically evaluate the effects of N_{ring} and the cyclic unit molecular weight ($M_{n,ring}$) on the efficiency of macro-rotaxane formation, mc-PBAs with different N_{ring} values ranging from 5 to 13 and $M_{n,ring}$ values of 19k and 32k were synthesized and prepared via the cyclopolymerization of NB–PBA$_{19k}$–NB and NB–PBA$_{32k}$–NB (Table 2, runs 3–6; Fig. S23–S30).

Synthesis of the reference samples

Linear PBA specimens with a high M_n content and grafted PBA were prepared as reference samples for mc-PBA (Scheme 1; Fig. S7–S10, S17, S18, S31, and S32). The linear PBA was designed to possess an M_n comparable to that of mc-PBA. In contrast, the graft PBA was designed such that the M_n of the graft side chain units was approximately half that ($M_{n,ring}/2$) of the cyclic units in mc-PBA, whereas the number of graft units was set to approximately twice the number of cyclic units ($2N_{ring}$). Linear PBA was synthesized via ATRP using a [BA]$_0$/[EBBiB]$_0$/[CuBr]/[CuBr$_2$]/[PMDETA] feed ratio of 5735 : 1.00 : 5.69 : 0.32 : 6.67, as described above. For the graft PBA, ω-norbornenyl-functionalized PBA (PBA-NB) was prepared by ATRP using ethyl 2-bromoisobutyrate

(EBiB) followed by treatment with exo-NB–COOH, and subsequent ROMP afforded the desired product. The resulting final products were denoted as Br–PBA$_{175k}$–Br and 19g-PBA$_{15k}$ based on their $M_{n,MALS}$ values. For 19g-PBA$_{15k}$, the prefix "19g" denotes the average number of graft units, which was calculated by dividing $M_{n,MALS}$ by the corresponding value for the macromonomer.

Synthesis and characterization of the mc-PBA-blended PBA network

Using mc-PBA specimens with various N_{ring} and $M_{n,ring}$ values, macro-rotaxanes were generated via photoradical polymerization in the presence of BA, together with ethylene glycol dimethacrylate (EGDM) as the cross-linker and 2,2-diethoxyacetophenone (DEAP) as the photoinitiator. The reaction was carried out in a quartz vessel under ultraviolet (UV) irradiation (352 nm) at room temperature for 1 h. mc-PBA was incorporated into a BA/EGDM/DEAP mixture (97 : 3 : 1, w/w/w) at loadings of 20, 40, and 60 wt%. It is anticipated that the PBA chains formed during radical polymerization thread through the mc-PBA rings. Subsequently, the cross-linking points, generated by the copolymerization with EGDM, act as end-capping agents to prevent dethreading of mc-PBA, thereby successfully constructing the target macro-rotaxane. Indeed, a control experiment without adding EGDM confirmed the dethreading of mc-PBA and linear PBA (Fig. S34). Assuming the successful formation of the macro-rotaxane, the mc-PBA rings would

remain trapped within the network, even after solvent swelling. The degree of macro-rotaxane formation was therefore assessed by determining the fraction of unextracted mc-PBA. Specifically, Soxhlet extractions with toluene were carried out for the 60 wt% mc-PBA-blended PBA networks over 4 days. The soluble fractions obtained by subsequent solvent evaporation were assumed to contain both free mc-PBA and the PBA sol fraction that was not incorporated into the network. To estimate the sol fraction, the same extraction procedure was applied to pristine PBA networks prepared without mc-PBA. As a result, 61.7 mg of the PBA sol fraction was extracted per gram of pristine PBA network (average of three independent experiments). Using this value, the fraction of mc-PBA trapped in the networks (%Trapped) was calculated to be 20–85% according to the following equation (Table 3, runs 1–7):

$$(\%\text{Trapped [\%]}) = \left\{ 1 - \frac{(\text{mass of soluble fraction [mg]}) - 61.7 \times [(\text{mass of mc-PBA-blended PBA network used in the test [g]}) - (\text{mass of added mc-PBA [g]})]}{(\text{mass of added mc-PBA [mg]})} \right\} \times 100\%$$

Despite sub-quantitative macro-rotaxane formation, the data demonstrated that threading took place to some extent, with the efficiency governed by the $M_{n,ring}$ and N_{ring} values of mc-PBA.

To further confirm macro-rotaxane formation, the same procedure was applied to the PBA networks prepared in the presence of 60 wt% Br–PBA$_{175k}$–Br and 19g-PBA$_{15k}$ (Table 3, runs 8 and 9). Owing to their acyclic nature, the added PBA chains are unable to mechanically interlock with the PBA network and should be completely extracted during solvent swelling. As expected, Soxhlet extraction revealed trapped fractions of <0.1% for the Br–PBA$_{175k}$–Br and 19g-PBA$_{15k}$-blended PBA networks. Focusing on the Br–PBA$_{175k}$–Br- and 5c-PBA$_{32k}$-blended PBA networks, it was found that although both additives had comparable M_n values, the added Br–PBA$_{175k}$–Br was completely extracted, whereas 57.3% of 5c-PBA$_{32k}$ remained trapped within the network (Table 3, runs 5 and 8). Furthermore, despite the similar molecular architectures and $M_{n,MALS}$ values of the 19g-PBA$_{15k}$ and 8c-PBA$_{32k}$-blended PBA

networks, 19g-PBA$_{15k}$ was completely extracted due to its acyclic structure, whereas 70.9% of 8c-PBA$_{32k}$ remained trapped within the network (Table 3, runs 6 and 9). These results confirm that the presence of a cyclic architecture is essential for entrapment within the network. Therefore, the observed retention of mc-PBA provides strong evidence for successful macro-rotaxane formation.

It is also possible that entrapment of high-molecular-weight mc-PBA arises from simple physical constraints within the network lattice rather than the expected macro-rotaxane formation. To examine this possibility, a series of PBA networks were prepared containing 12c-PBA$_{19k}$ (60 wt%) with varying cross-link densities. This was achieved by systematically altering the feed ratio of the EGDM cross-linker from 1 to 6 wt%. The theoretical molecular weights between the cross-linking points (M_c) determined by the feed ratio were ~9800, 3200, and 1600 for 1, 3, and 6 wt% EGDM, respectively. Subsequently, Soxhlet extractions were performed on the obtained PBA networks, and the trapped fraction was evaluated (Table 4 and Fig. 4a). The 12c-PBA$_{19k}$-blended PBA network prepared using 1 wt% EGDM exhibited a slightly lower trapped fraction (52.2%) than those prepared using 3 and 6 wt% EGDM, due to the increased number of network defects caused by the lower cross-link density. Nevertheless, all three samples exhibited similar trapped fractions (52.2–65.2%). In particular, the 12c-PBA$_{19k}$-blended PBA network prepared using 6 wt% EGDM exhibited a value similar to that of the network prepared using 3 wt% EGDM, despite the cross-link density being doubled and the physical constraints imposed on mc-PBA being significantly increased. These results confirm that mc-PBA formed macro-rotaxanes that dominated the trapping behavior within the PBA network.

To investigate the effect of N_{ring} on the efficiency of macro-rotaxane formation, the trapped fractions of a series of mc-PBAs with identical $M_{n,ring}$ values (32k) were also examined (Fig. 4b), revealing an increase in trapping with increasing

Table 3 Extraction tests performed on 60 wt% mc-PBA, Br–PBA–Br, and g-PBA-blended PBA networks[a]

Run	Additive	Mass of soluble fraction per g of network [mg]	%Trapped [%]
1	—	61.7 ± 8.0	—
2	8c-PBA$_{10k}$	337.2	20.4
3	34c-PBA$_{10k}$	259.8	41.0
4	12c-PBA$_{19k}$	169.2	65.2
5	5c-PBA$_{32k}$	198.4	57.3
6	8c-PBA$_{32k}$	147.4	70.9
7	13c-PBA$_{32k}$	96.4	84.6
8	Br–PBA$_{175k}$–Br	456.8	<0.1
9	19g-PBA$_{15k}$	456.8	<0.1

[a] Polymerization conditions: temperature, r.t.; BA/EGDM/DEAP = 97 : 3 : 1 (w/w/w); mixture of BA, EGDM, and DEAP/additive = 100 : 60 (w/w).

Table 4 Extraction tests performed on 12c-PBA$_{19k}$-blended networks with varying M_c values[a]

Run	Additive	BA/EGDM/DEAP (w/w/w)	M_c [b]	Mass of soluble fraction per g of network [mg]	%Trapped [%]
1	—	99 : 1 : 1	9800	115.4 ± 10.4	—
2	—	97 : 3 : 1	3200	61.7 ± 8.0	—
3	—	94 : 6 : 1	1600	34.5 ± 5.9	—
4		99 : 1 : 1	9800	251.8	52.2
5	12c-PBA$_{19k}$	97 : 3 : 1	3200	169.2	65.2
6		94 : 6 : 1	1600	169.7	60.6

[a] Polymerization conditions: temperature, r.t.; mixture of BA, EGDM, and DEAP/additive = 100 : 60 (w/w). [b] Determined from the BA/EGDM feed ratio.
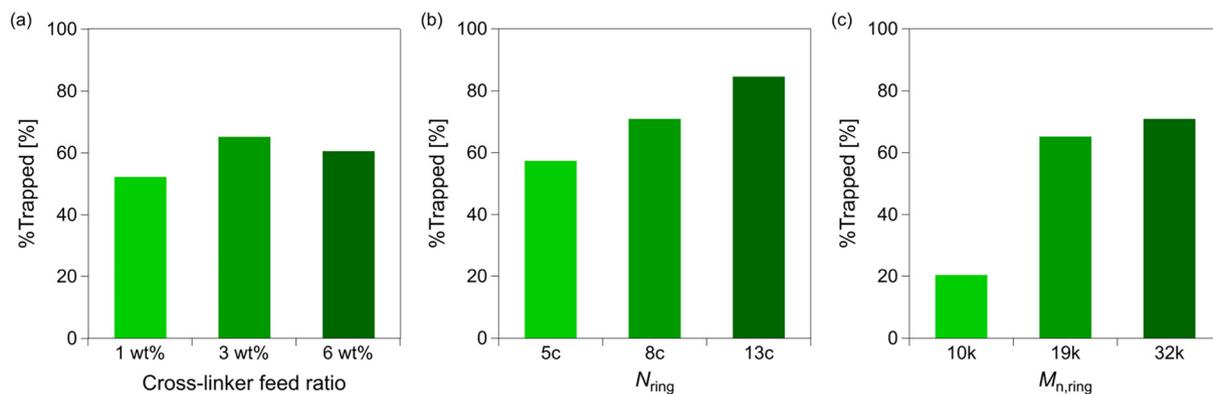
Fig. 4 Molecular parameters affecting trapping efficiency. (a) Effect of the cross-linking feed ratio on the trapping efficiency for the 60 wt% 12c-PBA$_{19k}$-blended PBA networks. (b) Effect of N_{ring} on the trapping efficiency for the 60 wt% 5c-PBA$_{32k}$-, 8c-PBA$_{32k}$-, and 13c-PBA$_{32k}$-blended PBA networks. (c) Effect of $M_{n,ring}$ on the trapping efficiency for the 60 wt% 8c-PBA$_{10k}$-, 12c-PBA$_{19k}$-, and 8c-PBA$_{32k}$-blended PBA networks.

N_{ring} (*i.e.*, from 57.3 to 84.6%). Subsequently, to assess the influence of $M_{n,ring}$, the trapped fractions of mc-PBAs with comparable N_{ring} (8–12) and different $M_{n,ring}$ values (10k, 19k, and 32k) were examined (Fig. 4c). Again, the trapped fraction increases with increasing $M_{n,ring}$, demonstrating that macro-rotaxane formation becomes more efficient with increasing N_{ring} and $M_{n,ring}$ values.

Our previous work demonstrated 100% trapping when macro-rotaxane formation was performed *via* end-cross-linking of linear PDMS in the presence of mc-PDMS with N_{ring} and $M_{n,ring}$ values of 6 and 26k, respectively. In contrast, in the present work, the maximum trapped fraction for mc-PBA remained around 85% even at high N_{ring} and $M_{n,ring}$ values. This could be attributed to several factors. First, the longer side chains of PBA compared with those of PDMS may have limited the network penetration in mc-PBA. Indeed, the entanglement molecular weight (M_e) of PDMS[37] (M_e = 10k) is lower than that of PBA[38] (M_e = 32k). Second, photoradical polymerization inherently produces networks with structural heterogeneity, such as dangling chains, which can partially form pseudo-macro-rotaxanes rather than true macro-rotaxanes. These factors reasonably account for the fact that the trapped fractions of the mc-PBA-blended PBA networks did not reach 100%.

Subsequently, swelling experiments were performed on the network samples after Soxhlet extraction (Table S1). The 60 wt% 5c-, 8c-, and 13c-PBA-blended PBA network samples exhibited approximately threefold M_c compared to the pristine PBA network. This result indicates that the mc-PBA interferes with the network formation process, leading to a decrease in the effective cross-link density and increased structural heterogeneity in the PBA network. These findings further support the observation that the trapped fraction did not reach 100%. On the other hand, a slight decrease in the M_c was observed with increasing N_{ring}. This trend suggests that as the N_{ring} increases, a greater number of network chains are threaded through the cyclic units, and the mc-PBA may partially act as additional cross-linking points.

Mechanical properties

Having established the successful formation of a macro-rotaxane network, attention was directed toward its damping performance to demonstrate its unique application potential. In various fields, such as automotive and construction engineering, vibration suppression using damping materials is essential for preventing fatigue failure and mitigating environmental noise. Liu *et al.*[39] recently demonstrated that the incorporation of a linear PBA into a PBA network significantly enhanced its damping properties, giving a tunable effective frequency range. In this system, the added linear polymer exhibited reptation behavior in the high-elastic region of the polymer network, leading to a substantial increase in energy dissipation. However, such linear additives could potentially leach out over time, compromising long-term stability. It was therefore envisaged that mc-PBA could yield a sustained damping performance due to topological trapping of the cyclic units within the macro-rotaxane architecture, effectively preventing leaching while maintaining the desired damping enhancement.

Thus, the effect of mc-PBA addition on the damping properties was investigated by dynamic viscoelastic measurements of PBA networks containing 20, 40, and 60 wt% 5c-PBA$_{32k}$ using a rotational rheometer with a parallel-plate geometry. Measurements were performed in the linear viscoelastic region (γ = 0.1%) (Fig. S36) and master curves of the storage modulus (G'), loss modulus (G''), and loss factor (tan δ) were created by time–temperature superposition using a reference temperature of 25 °C (Fig. 5). The tan δ value is a key parameter reflecting energy dissipation in the material. Focusing on the pristine PBA network, a distinct peak in tan δ associated with the glass transition was observed in the high-frequency region, whereas a rubbery plateau region originating from the cross-linked structure was evident in the low-frequency region. In the low-frequency region ($\omega \rightarrow 0$), G' decreased with increasing mc-PBA content, while tan δ increased. This decrease in G' was attributed to a decrease in PBA cross-link density due to the inter-
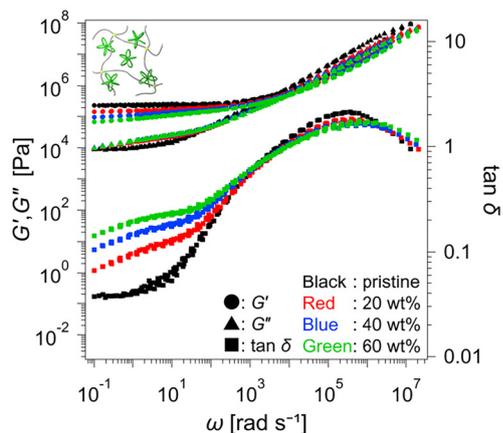
Fig. 5 Master curves of G', G'', and $\tan\delta$ at a reference temperature of 25 °C for the pristine PBA network (black), 20 wt% 5c-PBA$_{32k}$ (red), 40 wt% 5c-PBA$_{32k}$ (blue), and 60 wt% 5c-PBA$_{32k}$ (green)-blended PBA networks.

ference of mc-PBA with network formation and dilution of the PBA network fraction by the added mc-PBA. In contrast, the increase in $\tan\delta$ was ascribed to mc-PBA chain relaxation, which enhances energy dissipation within the network. These results clearly demonstrate that mc-PBA incorporation improves the damping properties of the PBA network, irrespective of macro-rotaxane formation. The increase in $\tan\delta$ upon the addition of this polymer is consistent with the results reported by Liu *et al.*, indicating that linear and cyclic polymers exhibit similar energy dissipation effects.

Subsequently, to clarify the influence of N_{ring} on the damping properties, PBA networks containing a series of mc-PBAs (60 wt%) with identical $M_{n,ring}$ values (32k) were investigated (Fig. 6a). It was found that $\tan\delta$ decreased as N_{ring} increased from 5 to 13, potentially due to the progressive increase in mc-PBA relaxation time with increasing N_{ring}. To support this interpretation, viscoelastic measurements were performed on neat mc-PBA, revealing that the crossover point of G' and G'' in the terminal flow region shifted toward lower frequencies. This shift confirms that the relaxation time of mc-PBA increases with higher N_{ring} values (Fig. 6b). The reduction in $\tan\delta$ could also be related to the increased fraction of mc-PBA trapped in the network at higher N_{ring} values (%Trapped = 57.3–84.6%). Macro-rotaxane-trapped mc-PBA is expected to exhibit more strongly restricted molecular motion than its untrapped counterparts. Consequently, the fluid-like behavior of mc-PBA is weakened, leading to suppressed energy dissipation in the network and a corresponding decrease in $\tan\delta$.

Finally, the potential of mc-PBA as a non-leaching additive was evaluated by examining changes in $\tan\delta$ before and after solvent washing to remove any untrapped mc-PBA. Dynamic viscoelastic measurements were conducted on networks blended with 60 wt% 13c-PBA$_{32k}$, which exhibited the highest trapping performance, and with 19g-PBA$_{15k}$, a control sample
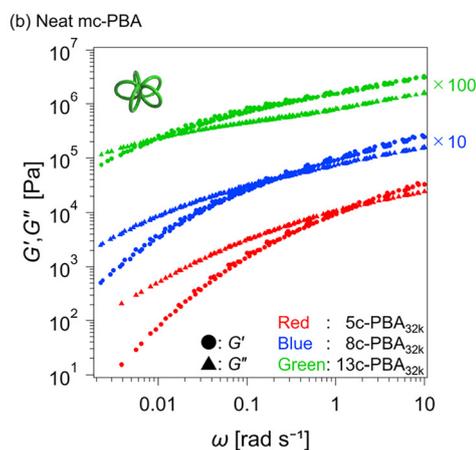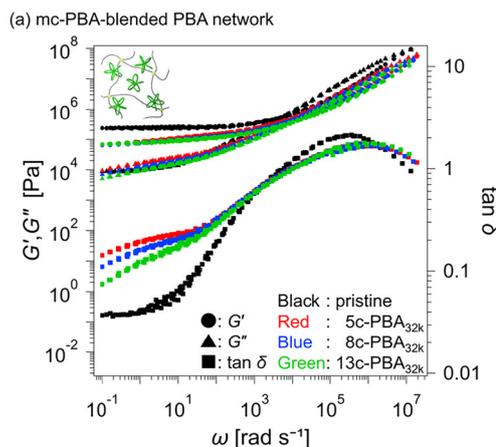

Fig. 6 (a) Master curves of G', G'', and $\tan\delta$ at a reference temperature of 25 °C for the pristine PBA network (black), 60 wt% 5c-PBA$_{32k}$ (red), 60 wt% 8c-PBA$_{32k}$ (blue), and 60 wt% 13c-PBA$_{32k}$ (green)-blended PBA networks. (b) Master curves of G' and G'' at a reference temperature of 25 °C for neat 5c-PBA$_{32k}$ (red), 8c-PBA$_{32k}$ (blue), and 13c-PBA$_{32k}$ (green).

without cyclic structures. Since the samples used for Soxhlet extraction were damaged during the process, alternative samples immersed in toluene for 2 d were employed. The calculated trapped fractions were 89.8 and <0.1% for the 13c-PBA$_{32k}$ and 19g-PBA$_{15k}$-blended PBA networks, respectively. As expected, the 13c-PBA$_{32k}$-blended PBA network exhibited similar $\tan\delta$ profiles before and after solvent washing, whereas the 19g-PBA$_{15k}$-blended PBA network showed a marked decrease in $\tan\delta$ after washing (Fig. S37). These findings clearly demonstrate that mc-PBA acts as an effective non-leaching additive in macro-rotaxane systems.

In addition, indentation tests were performed to investigate the effect of mc-PBA on Young's modulus (E) (Fig. S38 and Table S2). The E value was calculated from the initial loading region based on Hertzian contact theory. The results revealed that the E value decreased upon the addition of mc-PBA, which is attributed to a reduction in the effective cross-link density. Furthermore, the E value was found to depend on both the N_{ring} and the $M_{n,ring}$ of the added mc-PBA, indicating that the mechanical properties can be tuned through the molecular parameters of mc-PBA and its fraction.

Conclusions

Macro-rotaxanes were formed *via* the photoradical polymerization of BA and a cross-linker in the presence of mc-PBA. Unlike conventional approaches based on the cross-linking of end-functionalized linear polymers, this method allowed the monomer itself to be used as the solvent and did not require time-consuming procedures such as solvent casting, thereby enabling the rapid formation of polymer networks incorporating macro-rotaxanes. Notably, increasing both N_{ring} and $M_{n,ring}$ led to a maximum macro-rotaxane formation efficiency of 84.6%. The damping properties of the mc-PBA-blended PBA networks were subsequently evaluated to assess the applicability of mc-PBA as a functional material. The results revealed that $\tan\delta$ increased owing to the enhanced relaxation behavior of mc-PBA compared with that of pristine PBA network. Furthermore, the enhanced $\tan\delta$ was retained even after washing with toluene, demonstrating the potential of mc-PBA as a non-leaching additive. Overall, this synthetic methodology and systematic evaluation provide a foundation for extending the present approach to a wide range of radically polymerizable monomers for macro-rotaxane formation and functional material development.

Author contributions

Kotaro Ibe: investigation, writing – original draft, methodology, visualization, and data curation; Yamato Ebii: investigation and methodology; Minami Ebe: investigation and methodology; Kazushige Suzuki: investigation; Takayuki Kurokawa: investigation; Takuya Yamamoto: investigation and supervision; Feng Li: investigation and supervision; Takuya Isono: investigation, supervision, conceptualization, writing – review and editing, and funding acquisition; Toshifumi Satoh: supervision, conceptualization, writing – review and editing, and funding acquisition.

Conflicts of interest

There are no conflicts to declare.

Data availability

The data supporting this article have been included as part of the supplementary information (SI). Supplementary information is available. See DOI: https://doi.org/10.1039/d6py00144k.

Acknowledgements

References

1 J. Li, Y. Li, Y. Guo, J. Xu, J. Lv, Y. Li, H. Liu, S. Wang and D. Zhu, *Chem. – Asian J.*, 2008, **3**, 2091–2096.

2 G. De Bo, M. A. Y. Gall, M. O. Kitching, S. Kuschel, D. A. Leigh, D. J. Tetlow and J. W. Ward, *J. Am. Chem. Soc.*, 2017, **139**, 10875–10879.

3 J. J. Yu, L. Y. Zhao, Z. T. Shi, Q. Zhang, G. London, W. J. Liang, C. Gao, M. M. Li, X. M. Cao, H. Tian, B. L. Feringa and D. H. Qu, *J. Org. Chem.*, 2019, **84**, 5790–5802.

4 L. Chen, R. Nixon and G. De Bo, *Nature*, 2024, **628**, 320–325.

5 R. Barat, T. Legigan, I. Tranoy-Opalinski, B. Renoux, E. Péraudeau, J. Clarhaut, P. Poinot, A. E. Fernandes, V. Aucagne, D. A. Leigh and S. Papot, *Chem. Sci.*, 2015, **6**, 2608–2613.

6 G. Yu, Z. Yang, X. Fu, B. C. Yung, J. Yang, Z. Mao, L. Shao, B. Hua, Y. Liu, F. Zhang, Q. Fan, S. Wang, O. Jacobson, A. Jin, C. Gao, X. Tang, F. Huang and X. Chen, *Nat. Commun.*, 2018, **9**, 766.

7 Y. Okumura and K. Ito, *Adv. Mater.*, 2001, **13**, 485–487.

8 C. Liu, N. Morimoto, L. Jiang, S. Kawahara, T. Noritomi, H. Yokoyama, K. Mayumi and K. Ito, *Science*, 2021, **372**, 1078–1081.

9 K. Kato, M. Taniguchi and K. Ito, *Macromolecules*, 2023, **56**, 1810–1817.

10 P. R. Ashton, P. T. Glink, J. F. Stoddart, P. A. Tasker, A. J. P. White and D. J. Williams, *Chem. – Eur. J.*, 1996, **2**, 729–736.

11 C. Zhang, S. Li, J. Zhang, K. Zhu, N. Li and F. Huang, *Org. Lett.*, 2007, **9**, 5553–5556.

12 S. Y. Hsueh, K. W. Cheng, C. C. Lai and S. H. Chiu, *Angew. Chem., Int. Ed.*, 2008, **47**, 4436–4439.

13 A. Hashidzume, H. Yamaguchi and A. Harada, *Eur. J. Org. Chem.*, 2019, 3344–3357.

14 H. Ogino, *J. Am. Chem. Soc.*, 1981, **103**, 1303–1304.

15 R. S. Wylie and D. H. Macartney, *J. Am. Chem. Soc.*, 1992, **114**, 3136–3138.

16 A. N. Basuray, H. P. Jacquot de Rouville, K. J. Hartlieb, T. Kikuchi, N. L. Strutt, C. J. Bruns, M. W. Ambrogio, A. J. Avestro, S. T. Schneebeli, A. C. Fahrenbach and J. F. Stoddart, *Angew. Chem., Int. Ed.*, 2012, **51**, 11872–11877.

17 D. B. Amabilino, P. R. Ashton, V. Balzani, C. L. Brown, A. Credi, J. M. J. Fréchet, J. W. Leon, F. M. Raymo,

N. Spencer, J. F. Stoddart and M. Venturi, *J. Am. Chem. Soc.*, 1996, **118**, 12012–12020.

18 Q. S. Zong, C. Zhang and C. F. Chen, *Org. Lett.*, 2006, **8**, 1859–1862.

19 F. Huang, D. S. Nagvekar, C. Slebodnick and H. W. Gibson, *J. Am. Chem. Soc.*, 2005, **127**, 484–485.

20 D. Parisi, J. Ahn, T. Chang, D. Vlassopoulos and M. Rubinstein, *Macromolecules*, 2020, **53**, 1685–1693.

21 M. Kapnistos, M. Lang, D. Vlassopoulos, W. Pyckhout-Hintzen, D. Richter, D. Cho, T. Chang and M. Rubinstein, *Nat. Mater.*, 2008, **7**, 997–1002.

22 G. S. Grest, T. Ge, S. J. Plimpton, M. Rubinstein and T. C. O'Connor, *ACS Polym. Au*, 2023, **3**, 209–216.

23 M. Kruteva, M. Monkenbusch, J. Allgaier, W. Pyckhout-Hintzen, L. Porcar and D. Richter, *Macromolecules*, 2023, **56**, 4835–4844.

24 S. J. Clarson, J. E. Mark and J. A. Semlyen, *Polym. Commun.*, 1986, **27**, 244–245.

25 T. S. Stukenbroeker, D. Solis-Ibarra and R. M. Waymouth, *Macromolecules*, 2014, **47**, 8224–8230.

26 L. Garrido, J. E. Mark, S. J. Clarson and J. A. Semlyen, *Polym. Commun.*, 1985, **26**, 53–55.

27 L. C. Debolt and J. E. Mark, *Macromolecules*, 1987, **20**, 2369–2374.

28 B. R. Wood, S. J. Joyce, G. Scrivens, J. A. Semlyen, P. Hodge and R. O'Dell, *Polymer*, 1993, **34**, 3059–3063.

29 W. Huang, H. L. Frisch, Y. Hua and J. A. Semlyen, *J. Polym. Sci., Part A:Polym. Chem.*, 1990, **28**, 1807–1812.

30 T. J. Fyvie, H. L. Frisch, J. A. Semlyen, S. J. Clarson and J. E. Mark, *J. Polym. Sci., Part A:Polym. Chem.*, 1987, **25**, 2503–2509.

31 T. Isono, T. Sasamori, K. Honda, Y. Mato, T. Yamamoto, K. Tajima and T. Satoh, *Macromolecules*, 2018, **51**, 3855–3864.

32 M. Ebe, A. Soga, K. Fujiwara, B. J. Ree, H. Marubayashi, K. Hagita, A. Imasaki, M. Baba, T. Yamamoto, K. Tajima, T. Deguchi, H. Jinnai, T. Isono and T. Satoh, *Angew. Chem., Int. Ed.*, 2023, **62**, e202304493.

33 Y. Ebii, Y. Mato, F. Li, K. Tajima, T. Yamamoto, T. Isono and T. Satoh, *Polym. Chem.*, 2023, **14**, 3099–3109.

34 K. Hagita and T. Murashima, *Polymer*, 2021, **223**, 123705.

35 H. Marubayashi, M. Ebe, A. Imasaki, K. Fujiwara, N. Mashita, K. Hagita, T. Murashima, S. Mori, T. Isono, T. Satoh and H. Jinnai, *Polymer*, 2024, **292**, 126607.

36 N. D. Ogbonna, M. Dearman, C.-T. Cho, B. Bharti, A. J. Peters and J. Lawrence, *JACS Au*, 2022, **2**, 898–905.

37 L. J. Fetters, D. J. Lohse, D. Richter, T. A. Witten and A. Zirkel, *Macromolecules*, 1994, **27**, 4639–4647.

38 N. Jullian, F. Leonardi, B. Grassl, J. Peyrelasse and C. Derail, *Appl. Rheol.*, 2010, **20**, 33685.

39 J. Huang, Y. Xu, S. Qi, J. Zhou, W. Shi, T. Zhao and M. Liu, *Nat. Commun.*, 2021, **12**, 3610.